18.5% LASER-DOPED SOLAR CELL ON CZ P-TYPE SILICON

Adeline Sugianto[1], Jim Bovatsek[2], Stuart Wenham[1], Budi Tjahjono[1], Guangqi Xu[1], Yu Yao[1], Brett Hallam[1], Xue Bai[1], Nicole Kuepper[1], Chee Mun Chong[1] and Raj Patel[2]
[1]ARC Photovoltaics Centre of Excellence, University of New South Wales, Sydney, NSW 2052 Australia
[2]Spectra Physics, a division of Newport Corporation, Santa Clara, CA 95054, United States

ABSTRACT

For many years, the selective emitter approach has been well-known to yield cell efficiencies well above those achieved by conventional screen-printed cells. A simple and effective way of forming a selective emitter can be achieved by laser doping to simultaneously pattern the dielectric with openings as narrow as 8 μm, and create heavy doping beneath the metal contacts. In conjunction with laser doping, light-induced plating (LIP) is seen as an attractive approach for forming metal contacts on the laser-doped regions, without the need for aligning masks or other expensive, long laboratory processes. As laser-doping is gaining increasing interests in the PV industry, selection of the most appropriate laser and processing conditions is important to ensure high yields in a production environment. In this work, we have identified a suitable laser that enables good ohmic contacts for a wide range of laser scan speeds. Sheet resistances of laser-doped lines as low as 2 ohms/sq was achieved at a scan speeds of <1 m/s, while a sufficiently high doping (~20 ohms/sq) is still achievable at scan speeds up to 6 m/s. Optimization of the laser parameters in this work lead to a cell efficiency of 18.5% being achieved with the laser-doped selective emitter (LDSE) structure. The cell also has an excellent pseudo fill factor (pFF) of 82.3% and a local ideality factor *n* nearing unity. This indicates there is minimal laser-induced damage and junction recombination as a result of the laser doping process.

INTRODUCTION

With the long historical development of cell technologies on p-type Si combined with the complexity of realising a decent boron-doped emitter on n-type devices, p-type Si wafers are seen to continue dominating the world's solar cell production in the next few years. While the current market trends focus on the use of thinner wafers and high-efficiency cells to promote cost reduction, the concept of a "selective emitter" appears to be the most eagerly pursued among the emerging, high-efficiency cell designs [1].

The selective emitter approach offers a number of significant advantages that contribute to the superior cell performance levels achieved by technologies such as the Buried Contact Solar Cells, the semiconductor finger solar cell and the world-record holding Passivated Emitter and Rear Locally diffused solar cell [2,3,4]. The heavy doping facilitates reduced contact resistance between the metal and the silicon, and shields the high recombination velocity metal/silicon interface from the active regions of the cell. By restricting the heavy doping beneath the metal contacts, the remainder of the surface remains lightly doped and hence has a good blue response.

A particularly effective but simple way of achieving a selective emitter is by using laser doping. With this technique, openings in the dielectric layer are created and heavily doped simultaneously as the laser beam passes, i.e a single process step [5]. This technique therefore only imposes localised heating on the wafer to form heavily doped selective emitters, while sparing the remaining area from high temperature processes.

Laser doping for solar cell applications can be categorized into three processing types: (1) gas immersed laser doping (GILD) [6], (2) wet laser doping with liquids [7] and (3) dry laser doping with solid films which is also known as laser induced melting of pre-deposited impurity doping (LIMPID) [8,9]. A review by Colville reports that GILD and wet laser doping tend to impose challenges associated with complexity of the laser system, costs and throughput in a production environment [1]. Therefore, the dry laser processing (LIMPID) is currently seen as the most viable option for laser doping.

A careful selection of the "dry laser" and its operating parameters is therefore crucial to minimise any laser-induced damage that would otherwise have adverse impact on the cell performance [10]. Thus, this paper reports investigations into the suitability of various types of "dry lasers" for the laser doping process. Having identified the most suitable laser, laser parameters were varied to study characteristics of the laser-doped melt and optimized the laser doping process for that laser. Finally, efficiency results are reported for laser-doped selective emitter (LDSE) cells fabricated with the selected laser.

LASER SELECTION

This section compares the laser-induced damage that results from different types of "dry lasers". The main parameters being varied for these lasers are laser wavelength, Q-switch frequency and laser pulse length. The PCD Sinton lifetime tester was used to characterize the quality of the wafer prior to and following the laser doping process.

In this experimental work, a batch of 1 ohm.cm n-type CZ wafers were saw damage etched and alkali textured with a final thickness of 180 μm. N-type wafers were chosen as opposed to p-type wafers with n^+ emitters to separate any crystallographic defects from junction recombination effect that might arise following the laser doping process. Wafers were coated with a 75 nm SiNx layer with a refractive index of 2.0 and spin-coated with

978-1-4244-5892-9/10/$26.00 ©2010 IEEE

phosphoric acid spin-on dopant (SOD) 45% (w/v) at 3500 rpm for 30 s. The batch was then divided into five groups according to the different types of dry lasers (Table 1). Each group of wafers was laser-doped using the respective lasers, with a 1 mm busbar and 26 fingers spaced 1 mm apart. The best laser processing parameters for each type of laser were selected so the optimum melting of the silicon and the heaviest doping possible could be achieved with minimal material ablation. The corresponding sheet resistance values for the laser parameters used for each laser are outlined in Table 1. Subsequently, all wafers were thermally annealed at 350 °C for 5 min to recover any voltage losses following the laser doping process.

The wafers were characterized using the Sinton PCD lifetime tester after SiNx deposition, laser doping and thermal annealing steps. The implied Voc (iVoc) values for each wafer at each step were recorded and summarized in Table 1. Both voltage losses after LD and after anneal are calculated with reference to the voltage being measured after the SiNx deposition.

Table 1- Comparison of voltage loss for various types of "dry lasers" on samples after laser doping and after a low-temperature thermal anneal step

Laser	Laser λ (nm)	Scan speed (m/s)	Rsheet (ohms/sq)	Voltage loss (mV)	
				after LD	after anneal
A	1064	0.033	412	54.4	50
A*	1064	0.01	23	42.6	42.9
B	532	0.01	5	49	42
C	532	0.01	25	30.7	21.9
D	532	0.5	2	17.9	6.1

Note: * indicates that the laser beam is set out of focus

It can be seen from Table 1 that all lasers induce some amount of damage to the silicon wafer, although in some cases the voltage loss may originate primarily from the high recombination velocity surface created through the removal of the SiNx passivating layer in localized areas, rather than from crystallographic damage. Laser A and A* suffer from the largest voltage loss of >40 mV while Laser D induces the least damage with a voltage loss of ~18 mV following laser doping.

For any laser process, the absorption profile of the target material of the irradiating light is of utmost importance. For near-infrared 1064 nm light, there is significant penetration of the light to a depth of ~100 μm into the silicon [12]. Such deep penetration is exacerbated by thermal feedback problems, where the absorption coefficient of the infrared photons increases significantly with increases in temperature. Such a large volume of molten silicon yields a large amount of stress following rapid instant solidification. As seen in Table 1, the sheet resistance of lines scribed with Laser A is significantly large (412 ohms/sq). This implies that Laser A is highly likely to have caused a significant surface ablation that translates into a voltage loss of >40 mV. While de-focusing the 1064 nm laser beam (Laser A*) appears to significantly reduce the ablation and achieve a reasonably low sheet resistance (23 ohms/sq), major cracks are still observed in the melt due to the nature of the high absorption length of the 1064 nm wavelength (Figure 1). While 1064 nm laser systems are technologically mature, robust and very cost effective, the results from Laser A and A* demonstrate that they are unfortunately not suitable for LDSE processing.

Unlike the 1064 nm light, the 532 nm wavelength light optically irradiates the silicon to a depth of ~1 μm [11]. As a result, a significant portion of the volume requiring doping absorbs the laser irradiated energy. This accounts for an intrinsically-efficient process that is not solely dependent on heat conduction to achieve the desired junction depth of a few microns. Such a process minimizes any steep thermal gradients which would otherwise create unwanted damage in the laser-doped region. Therefore, Laser B, C and D are a more attractive option for LDSE processing. With a careful selection of laser parameters, Laser D from Spectra Physics was found to induce the smallest voltage loss and hence the least damage compared to the other 532 nm lasers (Lasers B and C). In addition, it also created the most heavily-doped melt at the fastest scanning speed (Table 1).

Another widely available choice of laser wavelength is the 355 nm UV lasers with a penetration depth of only about 10 nm into the silicon [11]. Any applied laser power is absorbed in such a shallow layer, requiring very little energy to melt the silicon. Reports also support the suitability of the 355 nm lasers for laser doping application [1]. However, significant heat conduction is required to achieve the desired junction depth for LDSE cells, and hence extended dwell times may be required. The total reliance on heat conduction for deep junction formation would tend to counteract somewhat the efficiency gain of the strong optical absorption, for example by the 532 nm laser. Furthermore, the suitable 355 nm laser systems for LDSE applications are relatively expensive in terms of both initial and ownership costs, and generally have less robust optics compared to the 532 nm lasers [12].

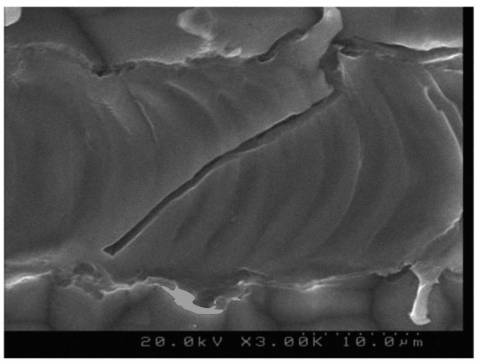

Figure 1 SEM image of a laser-induced crack in the laser-doped melt formed by Laser B.

It is also interesting to see from Table 1 that the voltage loss after laser doping is reduced for all samples following the low-temperature thermal anneal. This

possibly results from restoring the hydrogen passivation to nearby regions that lost hydrogen during laser doping. Alternatively, a fraction of the damage may be recovered during the anneal process through the release of hydrogen atoms in the SiNx layer (hydrogenation). Samples that suffer from severe laser-induced defects (Laser A and A*) do not benefit significantly from the annealing, with voltage loss above 40 mV. On the other hand, samples with minimum laser-induced damage experienced a significant improvement in iVoc following the thermal annealing step. The best improvement was achieved for samples scribed with Laser D with a voltage loss of only ~5 mV.

In summary, it was concluded that Laser D from Spectra Physics is the most suitable laser for LDSE processing from the standpoint of minimal damage, low-cost and high-volume manufacturability. This laser was therefore selected for the remaining experiments reported in this paper.

SPECTRA PHYSICS LASER

The Spectra Physics Millennia Prime is a Diode-Pumped Solid State (DPSS) laser system with high-quality TEM_{00} mode beam output and good focusing ability (M^2 <1.1). More technical specifications are listed in Table 2. Considering the large number of fingers and busbars required for a solar cell, high process throughput is best achieved with a fast beam-scanning system as opposed to a moving linear X-Y table. However, high optical intensities must then be generated to induce proper melting of the silicon to compensate for short dwell time due to fast beam scanning. This can be achieved by a careful design of the laser optics (Figure 2) to produce a reduced focused beam spot size.

Table 2 Listing of Millennia laser specifications

Laser Characteristic	Value
Laser crystal	Nd:YO_4
Output power (set value)	15 W
Wavelength	532 nm
Beam diameter ($1/e^2$)	2.3 mm
Power stability	± 1%
Beam pointing stability	≤2 μrad/°C
Noise	<0.04% rms

IMPACT OF VARYING LASER PARAMETERS ON THE CHARACTERISTICS OF THE LASER-DOPED MELT

Basic Steps of Laser Doping

The focused laser beam is directed onto the surface and scanned at high speed across the wafer surface in the regions where plating is desired. The 532 nm laser beam transmits through both the phosphoric acid spin-on dopant (SOD) and the SiNx coating and into the silicon. The beam penetrates optically to a depth of ~1 μm before being substantially absorbed. With sufficient laser intensity and dwell-time, the silicon is brought to its melting temperature while the phosphorus SOD is simultaneously vaporized.

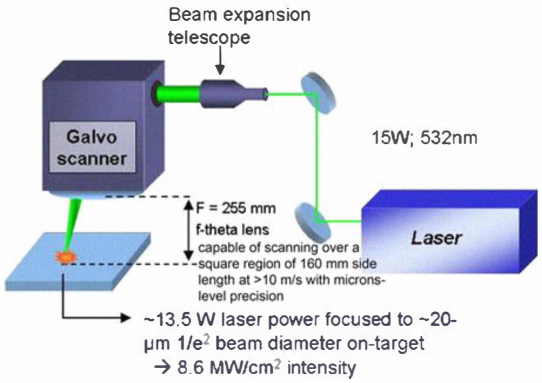

Figure 2 Schematic of the optical system used for the experimental work

With molten silicon conjoined with the phosphorus-laden vapor, heavy doping of the selected emitter region is achieved.

Melt width

With the 20-μm ($1/e^2$ intensity) optical spot size used in this experiment, the resultant laser-doped features are typically 8-15 μm wide. The discrepancy between the focused beam diameter (20 μm) and the laser-doped feature width is a limiting affect caused by the Gaussian intensity distribution of the laser beam. This means moving away from the centre of the beam, there is a gradually decreasing intensity which eventually becomes too low to melt the silicon.

Referring to Figure 3, the optical beam diameter of ~20 μm corresponds to the ~1 MW/cm^2 intensity contour for the 13.5 W power level used in this work. However, there is an insufficient amount of energy at this intensity level to melt the silicon at the high scan speeds realized in this work. Moving towards the centre of the beam, the intensity increases according to the Gaussian spatial power distribution. In between the boundary and the centre of the beam, there will be an intensity level that is just sufficient to melt and dope the silicon for a given scan speed.

As seen in Figure 4, faster scan speed results in a narrower line width. A line width as narrow as 8 μm is achievable at scan speed of 7 m/s. Faster scan speeds lead to a shorter dwell time of the laser beam, and hence require higher intensities to melt the silicon. As these higher intensities exist nearest to the centre of the beam, it therefore follows that higher scan speeds will result in narrower melt widths. On the other hand, at slower speeds, the dwell time of the laser beam on the silicon material is longer. This allows heat to accumulate under the beam and radiate outwards, resulting in a wider melt region.

By matching the intensity contours in Figure 3 to the laser-doped feature widths typically achieved (~8-15 μm) in Figure 4, the corresponding intensities fall in the range of 2-6 MW/cm^2 for the range of scan speeds 2 – 10 m/s. It should be noted here that the threshold for melting is believed to be sensitive to material variations such as

surface texture and dielectric layer constituency since these will affect both the optical coupling of energy to the material and the mechanisms of heat transfer. As such, these numbers are considered highly approximate.

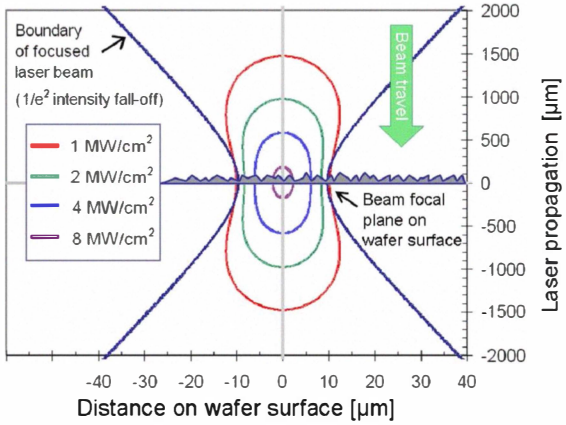

Figure 3 Boundary of focused laser beam and intensity contours in the vicinity of the silicon surface

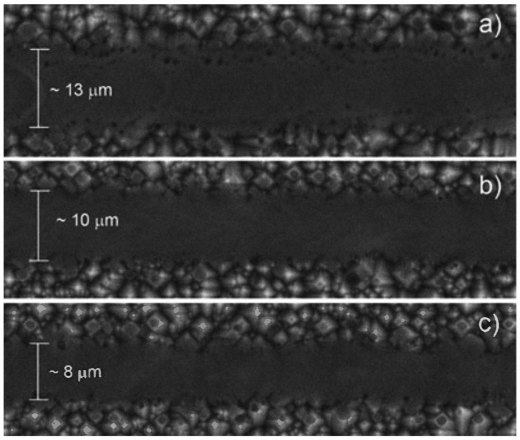

Figure 4 Top view SEM images of laser-doped lines scribed at scan speed of a) 2 m/s, b) 4 m/s and c) 7m/s

Doping profile and Sheet Resistance

The dopant concentration and the junction depth are dependent on two primary parameters, namely the incident optical intensity (laser output power per unit area) and the scan speed of the focused laser beam over the silicon material. Typical doping profiles of the laser-doped lines are shown in Figure 5 for various scan speeds. While a complete set of sheet resistance values for varying laser power and scan speeds are summarized in Figure 6. From Figure 5, it can be seen that dopant concentration and junction depth increases with decreasing scan speed, resulting in lower sheet resistances (Figure 6). A sheet resistance as low as 2 ohms/sq is achieved using an output power of 15 W and a scan speed of 0.5 and 1 m/s, while 20 ohms/sq and 40 ohms/sq doping are achievable at 6 m/s and 10 m/s respectively.

At slow scan speeds, thermal accumulation builds up in the silicon with the increased irradiation time per unit area, allowing a larger number of phosphorus dopant atoms to be incorporated into the molten region. In addition, reduced scan speeds results in higher surface concentrations due to the extended interaction time of the phosphorus with the molten silicon. Similar trends are also observed for increasing laser power.

However, extremely slow scan speeds are not desirable as it appears to cause material ablation to a certain extent. This is supported by the increasing sheet resistance values in Figure 6 when scan speeds below 0.5 m/s are used.

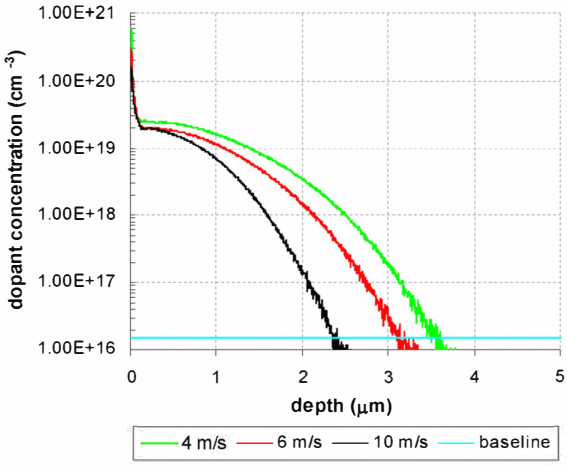

Figure 5 SIMS profiles for laser-doped lines scribed at 4, 6 and 10 m/s at 15 W with a p-type background doping level of ~1.5E+16 cm^{-3}

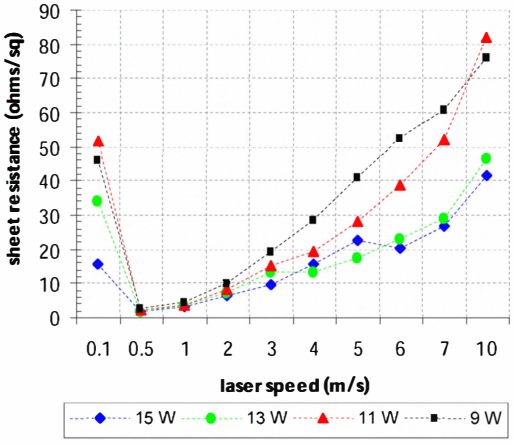

Figure 6 Comparison of sheet resistance values for various laser scan speeds and set output power. Generally acceptable sheet resistance values are around < 30 ohms/sq to facilitate good ohmic contacts.

Laser-induced Damage

To assess the laser-induced damage, a batch of textured, 1 ohm.cm n-type CZ samples was prepared as described previously in the "Laser Selection" section. The batch was divided into two categories: 1) with and 2) without the phosphoric acid SOD. Samples from each

group were laser-doped with 15 W laser power and scan speeds ranging from 0.1 m/s to 10 m/s, followed by a thermal anneal step at 350 °C for 5 min. To quantify any laser-induced damage that may have formed, the iVoc of each sample was measured after each of the following steps: 1) SiNx deposition; 2) laser doping and 3) low temperature thermal anneal. The results are presented in Figure 7 below.

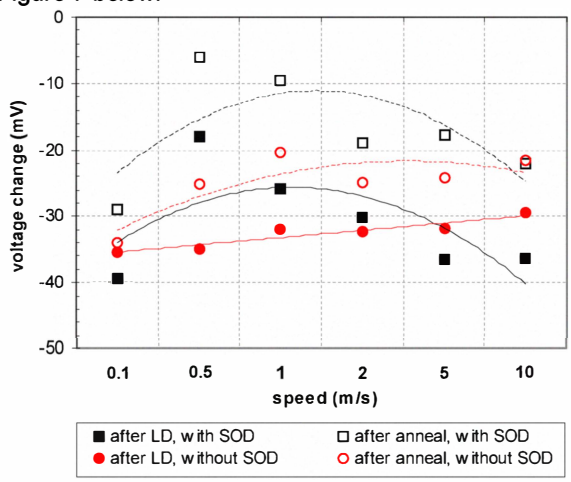

Figure 7 Comparison of voltage loss for various laser scan speeds before and after thermal anneal, on samples with and without SOD

As seen in Figure 7, for samples without SOD, decreasing laser scan speeds causes an increasing voltage loss. The longer dwell time with the reduced scan speeds potentially causes stronger thermal gradients upon solidification. Therefore, it increases the potential for undesirable damage to the silicon. On the other hand, for samples with SOD, the voltage loss strongly depends on the degree of doping in the laser-doped line. In reference to Figure 6, samples with the most heavily doped lines scribed at 0.5 m/s have the smallest voltage loss of ~18 mV after laser doping and ~5 mV after annealing. This is most likely due to the ability of the heavy doping to shield the active regions of the device from the high recombination velocity surface exposed following silicon nitride removal. This also helps explain why a more significant improvement in iVoc is observed on samples scribed with SOD than those without SOD.

As observed previously, samples that suffer from severe laser-induced damage, which in this case refers to lines scribed at 0.1 m/s without SOD, hardly benefit from the annealing process. The improvement in iVoc after annealing progressively increases with scanning speed where less damage is created.

LDSE CELL FABRICATION

A batch of textured, 1 ohm.cm p-type CZ wafers with 100-120 ohms/sq n^+ emitter diffusion and rear-etched back surfaces, was coated with a front dielectric layer as an antireflection coating and subsequent plating mask. Wafers were Al screen-printed and spike fired at 860 °C for 3 s. A layer of phosphoric acid 45% (w/v) SOD was spun onto each wafer at 3500 rpm for 30s. The wafers were laser-doped using the Spectra Physics Millennia Laser (Table 2) at 15 W with various scan speeds: 0.5, 2 and 5 m/s, with a 1 mm finger spacing pattern. With respect to the ten times difference in scan speeds, a 5-inch wafer for example can be processed in 5-6 s at 5 m/s compared to ~1 min at 0.5 m/s.

Prior to plating, wafers were deglazed in HF 1% for 30s. The plating process was carried out using an LIP method substantially as described by Durkee [13]. A thin layer of Ni was deposited into the laser-doped lines and the wafers were subsequently sintered at 400 °C in a N_2 environment, followed by Cu LIP to form the bulk of the metal contacts.

Table 3 Light IV results for LDSE cells scribed at various scan speeds

Scan speed (m/s)	Voc (mV)	Jsc (mA/cm^2)	FF (%)	Efficiency (%)
0.5	635	37.4	78	18.5
2	631	37.3	78	18.4
5	622	37.8	77	18.2

As seen in Table 3, the highest efficiency of 18.5% was achieved using a scan speed of 0.5 m/s. Suns-Voc measurements performed for this cell revealed a pFF of 82.3% and an *n at* P_{MPP} of 1.07, showing little laser-induced damage or junction recombination associated with the laser doping process. The use of LIP also minimizes the chance of metal puncturing through the p-n junction following Ni sinter, as illustrated in Figure 8. However, a A decent FF of above 77% was demonstrated regardless of scan speed, showing that uniform Ni plating and an excellent Cu aspect ratio (25 μm wide x 7 μm high) were achieved, as shown in Figure 9. The Voc decreased slightly with faster scan speeds. This observation is consistent with the trend observed in Figure 7. In addition, higher scan speeds produce shallower junctions that are more prone to metal shunting. Such shunts increase the dark saturation current due to increased metal/Si area. At scan speeds of 5 m/s, the change in Voc accelerates and is observed to fall below 630 mV. Such a voltage loss might have been exacerbated by the use of higher resistivity wafers due to the variability of the p-type wafer supply. However, a comparably high Jsc and FF were achieved on this sample.

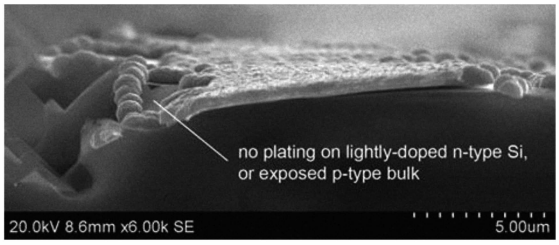

Figure 8 SEM image of a cross-section of uniformly grown Ni deposits using LIP

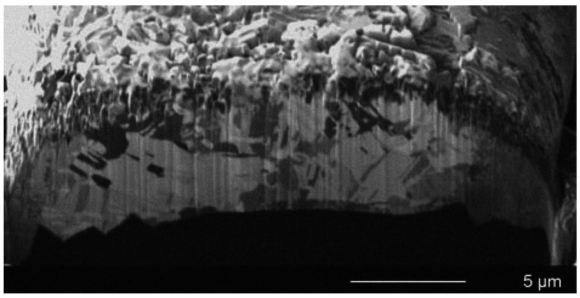

Figure 9 FIB image of a cross-section of LIP copper (tilted at 44°).

The spectral response curve of the best cell (Figure 10) shows a good blue response which translates to a comparatively high Jsc (> 37 mA/cm^2) when compared to a screen-printed cell. A very high internal quantum efficiency (IQE) value nearing unity was maintained from 400nm to 950nm. However, a slight drop in the IQE was observed in the short wavelength range, indicating that the front surface passivation can be further improved.

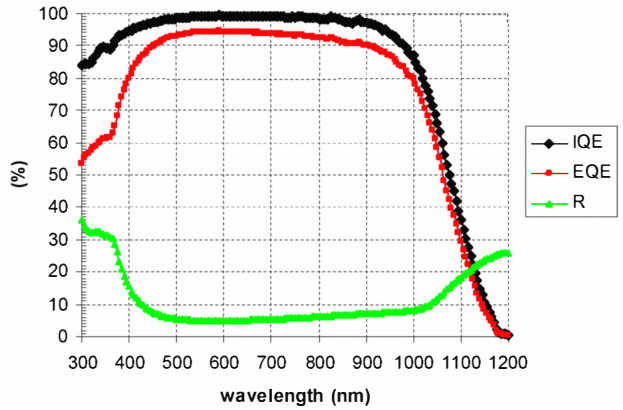

Figure 10 Spectral response curves of the 18.5% LDSE cell

CONCLUSION

As the selective emitter technology promises to provide high-efficiency cell designs, a simple, high-volume and cost-effective technology to fabricate selective emitter cells must be developed. Through careful selection of the laser technology and process parameters, we have demonstrated such an effective and simple laser doping technique to form selective emitters. Using a high power 532 nm Spectra Physics Millennia Prime laser system, an impressive LDSE cell efficiency of 18.5% was successfully demonstrated on commercial grade p-type CZ silicon using the high power. The laser system is able to provide heavy doping below 20 ohms/sq while maintaining a high scanning speed up to 6 m/s, with minimal damage being induced on the silicon surface. A pFF of 82.3% and *n* nearing unity were achieved, showing that virtually no laser-induced damage or junction recombination was involved. Further optimization work such as improved surface passivation appears to have the potential to further increase the efficiency to 19%.

ACKNOWLEDGEMENT

The authors would also like to acknowledge the financial assistance of the Australian Research Council, Suntech Power and Sunrise Global Solar Energy for funding this project.

REFERENCES

[1] F. Colville, "Laser-assisted Selective Emitters and the Role of Laser Doping", *Technical papers on Cell Processing in the fifth ed. of Photovoltaic International Magazine*, 2010, pp.1-6.

[2] S.R. Wenham and M.A. Green, "Buried Contact Solar Cells", *Patent No. 570309*, 1985: Australia.

[3] L. Mai, et al., "New Emitter Design and Metal Contact fro Screen-Printed Solar Cell Front Surfaces", *Fourth IEEE World Conference on PVSEC,* 2006, pp. 890 – 893.

[4] J. Zhao, et al.," 24% Efficienct PERL Silicon Solar Cell: Recent Improvements in High Efficiency Silicon Solar Cell Research", *SOLMAT* **41-42**, 1996, p.87 – 99.

[5] S.R. Wenham and M.A. Green, "Self Aligning Method for forming a Selective Emitter and Metallization in a Solar Cell", *Patent No. 6429037*, 2002: United States.

[6] G. Turner et al., "Solar Cells Made by Laser-induced Diffusion Directly from Phosphine Gas", *Appl. Phys. Lett.* **39**, 1981, pp. 967 – 969.

[7] D. Kray et al., "Laser Chemical Processing – a Versatile Tool for Microstructuring Applications", *Appl. Phys. A* **93**, 2008, pp. 99 – 105.

[8] U. Besi-Vetrella et al., "Large Area Screen Printed Silicon Solar Cells with Selective Emitter Made by Laser Overdoping and RTA Spin-on Glasses", *Twentysixth IEEE PVSC*, 1997, pp.135 – 138.

[9] B.S. Tjahjono, et al., "High Efficiency Solar Cell Structures Through the Use of Laser Doping", *Twentysecond EUPVSEC*, 2007, pp.966 – 969.

[10] A. Sugianto, et al., "Impact of Laser-induced Defects on the Performance of Solar Cells using Localised Laser-doped Regions beneath the Metal Contacts", Twentysecond EUPVSEC, 2007, pp.1759 - 1762.

[11] S.M. Sze, "Physics of Semiconductor Devices", John Wiley and Sons, 1981: New York.

[12] D. Clark. "Lasers in Solar Cell Production", Photonics Spectra. October 2009, United States: Lauren Publishing.

[13] Lawrence F. Durkee, "Method of Plating by Means of Light", Patent No. 4144139, 1979: United States.